Nuclear Engineering and Design 306 (2016) 52–58

Contents lists available at ScienceDirect

Nuclear Engineering and Design

journal homepage: www.elsevier.com/locate/nucengdes

Evaluation of the mechanical performance of silicon carbide in TRISO fuel at high temperatures

Nadia Rohbeck *, Ping Xiao *

School of Materials, University of Manchester, Grosvenor Street, M13 9PL Manchester, United Kingdom

ARTICLE INFO

Article history:
Received 10 March 2015
Received in revised form 29 October 2015
Accepted 4 May 2016
Available online 22 June 2016

ABSTRACT

The HTR design envisions fuel operating temperatures of up to 1000 °C and in case of an accident even 1600 °C are conceivable. To ensure safety in all conditions a thorough understanding of the impact of an extreme temperature environment is necessary. This work assesses the high temperature mechanical performance of the silicon carbide (SiC) layer within the tristructural-isotropic (TRISO) fuel particle as it poses the main barrier against fission product release into the primary circuit. Therefore, simulated fuel was fabricated by fluidized bed chemical vapour deposition; varying the deposition conditions resulted in strongly differing SiC microstructures for the various samples. Subsequently the TRISO particles were annealed in inert atmosphere at temperatures ranging from 1600 °C up to 2200 °C. Scanning electron microscopy and Raman spectroscopy showed that strong disintegration of the SiC layer occurred from 2100 °C onwards, but initial signs of porosity formation were visible already at 1800 °C. Still, the elastic modulus and hardness as measured by nanoindentation were hardly impaired. After annealing stoichiometric SiC coatings showed a reduction in fracture strength as determined by a modified crush test, however the actual annealing temperature from 1600 °C to 2000 °C had no measureable effect.

Furthermore, a technique was developed to measure the elastic modulus and hardness in situ up to 500 °C using a high temperature nanoindentation facility. This approach allows conducting tests while the specimen and indenter tip are heated to a specific measurement temperature, thus obtaining reliable values for the temperature dependent mechanical properties of the material. For the SiC layer in TRISO particles it was found that the elastic modulus decreased slightly from room temperature up to 500 °C, whereas the hardness was reduced more severely to approximately half of its ambient temperature value.

1. Introduction

The HTR fuel design foresees the application of a composite fuel, where the fissionable material is fully enclosed by successive layers of pyrolytic carbon and silicon carbide (SiC). Within each tristructural-isotropic (TRISO) fuel particle the SiC coating poses the main barrier against fission product release into the primary circuit, hence retaining its mechanical integrity in all conditions is a vital safety concern. Envisioned fuel operating temperatures for the HTR are up to 1000 °C, but in case of an accident 1600 °C can be reached. Even though this benchmark temperature has been established as a limit for safe fuel performance the exact impact on the physical properties of the fuel at this threshold temperature and beyond are not unambiguously clear (Verfondern, 2011). Approaches have been developed to assess the mechanical properties of coatings in TRISO fuel (due to the specimens' spherical shape and low sample volume many established tests are not feasible) and a range of studies report mechanical data of SiC coatings.

For improving the fuel performance several properties of the SiC coating layers are of interest. Firstly, the fracture strength, which is commonly evaluated by a crush test, was found to vary strongly with values ranging from a few hundred MPa up to more than a thousand MPa in some cases (Ogawa and Ikawa, 1981; Hong et al., 2007; Byun et al., 2010). Secondly, nanoindentation measurements giving the elastic modulus and hardness also found large variations for different fuels (Hosemann et al., 2013; López-Honorato et al., 2008, 2009). Not all these studies report the exact parameters used in the fabrication process, even though those strongly influence the microstructure of the deposited coatings, which in turn determines the mechanical properties. This further complicates making general conclusions about the best deposition conditions.

Several researchers have addressed the high temperature performance of SiC in TRISO, but the available data is still limited up

* Corresponding authors.
E-mail addresses: nadia.rohbeck@manchester.ac.uk (N. Rohbeck), p.xiao@manchester.ac.uk (P. Xiao).

http://dx.doi.org/10.1016/j.nucengdes.2016.05.040
0029-5493/

until today (van Rooyen et al., 2012, 2010; Zhang et al., 2013; Hancke et al., 2013; Minato and Fukuda, 1991; Ikawa et al., 1978; Rooyen et al., 2012). However, these prior studies suggest that SiC is capable of retaining its mechanical integrity even during short term exposure to temperatures exceeding the current benchmark of 1600 °C. A better understanding of the governing processes at these extreme conditions would be useful in the development of the fuel design and improve current modelling codes.

Hence, here a modified crush test (Hong et al., 2007) and nanoindentation were used to evaluate simulated fuel annealed at 1600 °C to 2200 °C and extensive microstructural characterisation was executed to develop a better understanding of the related physical phenomena. Furthermore, an approach was developed to measure the evolution of elastic modulus and hardness with temperature in situ up to 500 °C by high temperature nanoindentation. These are the first results of this kind and offer the opportunity to assess the mechanical properties closer to the actual operating conditions.

2. Materials and methods

2.1. Sample fabrication

Simulated TRISO fuel has been fabricated within a fluidized bed chemical vapour deposition (FBCVD) furnace using zirconia kernels with a nominal diameter of 500 μm diameter as a substrate. Firstly two layers of carbon were fabricated: a highly porous (buffer) and a dense pyrolytic carbon (IPyC) coating. Subsequently the silicon carbide coating was deposited using methyltrichlorosilane (MTS) as a precursor that was picked up and diluted by hydrogen (H_2). The exact deposition conditions are listed in Table 1; the temperature was varied strongly to obtain different SiC microstructures, while the MTS concentration had to be adjusted to suppress porosity formation. No outer pyrolytic carbon (OPyC) layer had been produced to allow a better comparison of the individual SiC sample performance.

Batches of sample 1, 2 and 3 were placed inside a graphite crucible and covered with a lid. Thermal treatment was executed in low-pressure (2 mbar) argon atmosphere with maximum temperatures from 1600 °C to 2100 °C that was held constant for 1 h. Annealing duration at 2200 °C was 15 min.

2.2. Sample characterisation

Samples were embedded into copper containing resin and polished to the approximate cross-section. Scanning Electron Microscopy (SEM) and Electron backscatter diffraction (EBSD) mapping were conducted using a Quanta FEG 650 (FEI). Raman Spectroscopy (He-Ne laser line in a Renishaw 1000 Raman System) was executed either directly on the sample surface or on the polished specimen cross-section. X-ray diffraction (XRD) patterns were collected using a Philips PW 1830 XRD instrument with a $CuK_{\alpha 1}$ radiation source. Therefore the intact samples had been fixed onto a single crystal silicon substrate with silicon paste.

The fracture strength was determined by applying the modified crush test approach as proposed by Hong et al. (2007). Around 30 samples were used for each sample and condition. Nanoindentation tests at room temperature were conducted using a Nanoindenter XP (MTS systems) and the measurements at elevated temperature were performed with a MicroMaterials (UK) system. Measurements were taken on the polished cross-section of the particles to either a penetration depth of 500 nm or 100 mN maximum load depending on the system. Both facilities are equipped with a diamond indenter tip of Berkovich shape and analysis was done by applying the Oliver-and Pharr-method (Oliver et al., 1992). The MicroMaterials facility uses an individually heated indenter tip and the sample is mounted onto a hot stage. The equipment is situated inside an atmospheric chamber, which was filled with argon for tests at 300 °C and above. Tests were conducted on sample 1 and a thin disk cut from a bulk CVD piece of SiC (Rohm & Haas, Dow Chemical Company).

3. Results and discussion

Thermal treatment of the samples led to visible changes in their appearance and detectable weight loss from 2000 °C onwards.

3.1. Microstructural evolution with temperature

SEM characterisation revealed a similar grain morphology in sample 1 and 2 with a faceted surface consisting of features of several micron size. The polished cross-section shows grains growing radially with the deposition direction (Fig. 1a). The much faster deposition rate used for sample 3 led to the formation of a hemispherical granular surface structure and the grains as seen in the cross-section are strongly elongated, thin and of equal size throughout the coating (Fig. 1d).

In the cross-section of all three samples the development of pores was visible after annealing at temperatures from 1800 °C or beyond and from 2100 °C onwards the disintegration of the SiC was so severe that layer thinning occurred (Fig. 1b). After annealing above 2000 °C the formation of SiC crystals on the sample surface was noticed (Fig. 1c) and at even higher treatment temperatures the complete SiC layer had migrated in some specimen exposing the underlying carbon coating. In sample 3 the formation of large precipitates in the SiC coating's cross-section was detected after annealing temperatures of 1800 °C and above (Fig. 1e). These observations were attributed to an evaporation-precipitation mechanism occurring in SiC at temperatures of 1600 °C and above. Evaporation sets in on the SiC grains causing porosity formation. The vapour phase migrates along grain boundaries and partly precipitates on the surface forming new large SiC crystals. The porosity was measured from SEM micrographs taken of the polished

Table 1
Sample deposition conditions and microstructural characteristics.

Sample ID	Furnace reference temperature* (°C)	Coating thickness (μm)	Deposition rate (μm/min)	MTS concentration (%)	H_2 flow rate (l/min)	Grain morphology and impurities
Sample 1	1700	35	0.58	1.2	12	Fully crystalline and stoichiometric composition, increasing grain size along the deposition direction of the coating
Sample 2	1600	32	0.36	0.6	12.4	Crystalline with traces of amorphous silicon, similar grain morphology as sample 1, but minor porosity visible
Sample 3	1500	38	0.69	9	6	Reduced crystallinity of the SiC and presence of amorphous silicon; thin, elongated equiaxed grains

* The furnace reference temperature is measured outside the heating element; the actual temperature in the deposition zone is lower.

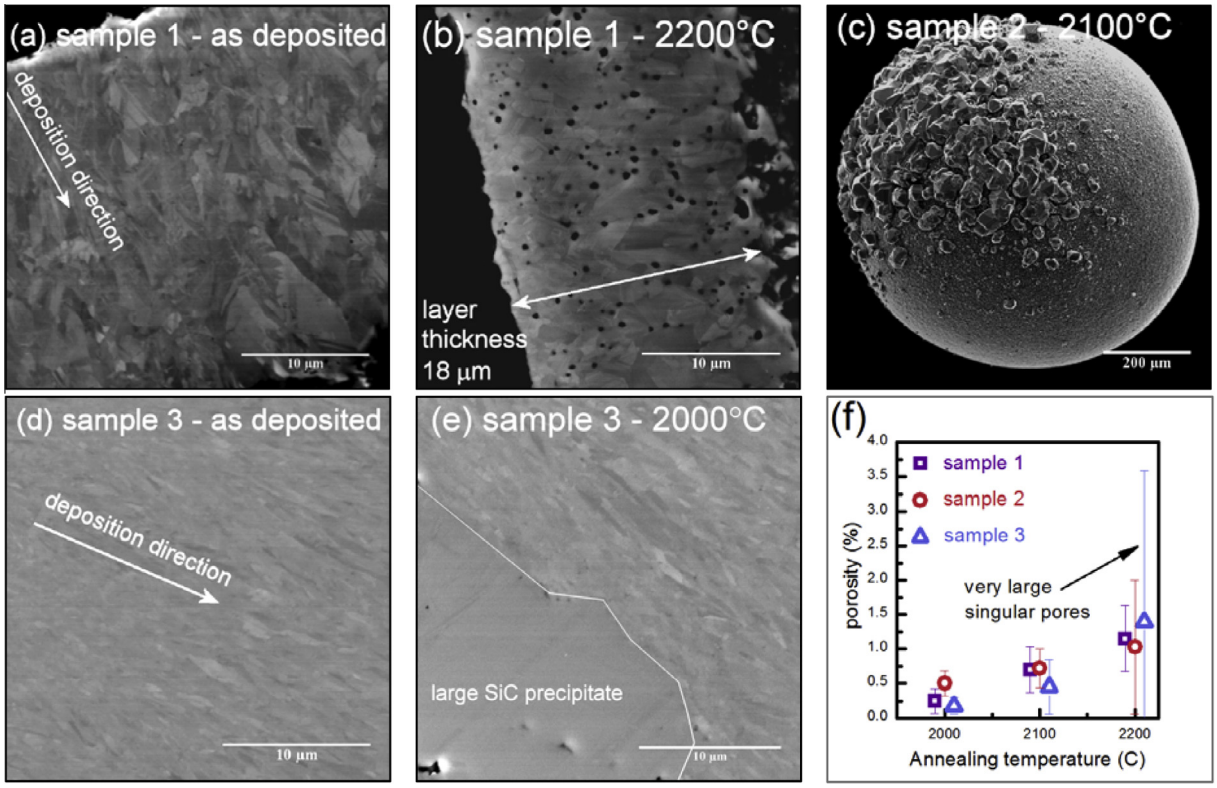

Fig. 1. SEM micrographs of annealed samples: (a) sample 1; (b) sample 1 after annealing at 2200 °C; (c) SiC crystal formation on TRISO particle surface after annealing at 2100 °C; polished cross-section of sample 3: (d) as deposited; (e) after annealing at 2000 °C; (f) porosity content in the SiC coatings after the highest annealing temperatures.

coating cross-section and increases exponentially with temperature as seen in Fig. 1f, however, the variations between the samples are minor. Even though porosity formation and crystal growth were seen in all samples the effect was more pronounced in sample 2 than 1 and most severe in sample 3. Similar observations had been made within previous studies. One publication reports the formation of porosity in SiC coatings when the TRISO fuel was subjected to annealing at 2000 °C (Zhang et al., 2013) and decomposition was obvious when annealing at 2100 °C (van Rooyen et al., 2010).

EBSD maps taken of sample 1 are displayed in Fig. 2 and results of the grain analysis are given in Table 2. The presence of numerous nano-sized grains in some locations presented difficulties when measuring the maps causing the indexing to fail completely in some areas (those were left white in the maps). Indexing was accomplished for β-SiC and the maps were noise reduced by standard zero solution extrapolation. The step size for the measurement was 0.1 µm and only grains with a diameter ⩾0.3 µm were taken into account in the statistical grain size analysis. Overall, grains were found to be on average of submicron size and exhibited a slightly elongated shape along the deposition direction. In direct comparison to EBSD maps of SiC coatings in the fuel of the AGR irradiation the microstructure of sample 1 here appears to be

Table 2
Grain statistics from EBSD measurements.

Sample 1	Mean grain diameter (µm)
As deposited (767)*	0.86 ± 0.56
2000 °C (1173)	0.74 ± 0.46
2100 °C (755)	0.88 ± 0.56

* Number of grain included in analysis.

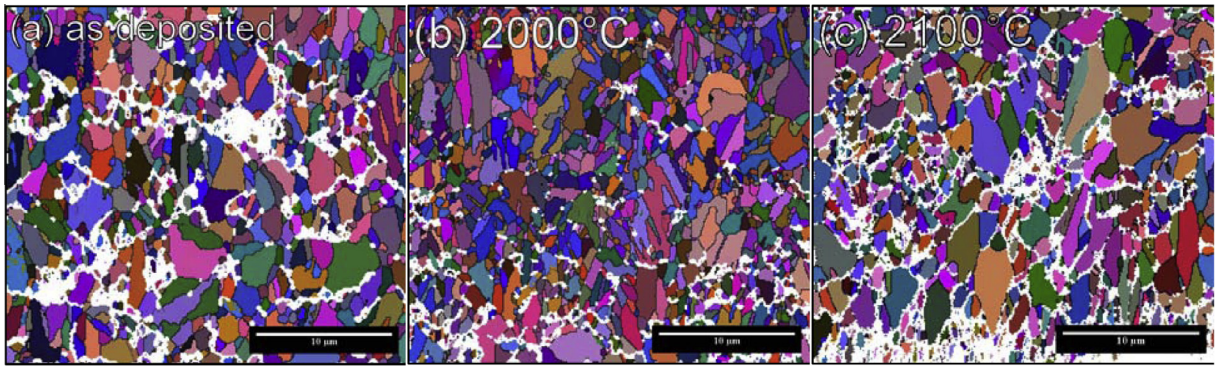

Fig. 2. EBSD maps taken of sample 1 (deposition direction from bottom to top): (a) as deposited; and annealed at (b) 2000 °C and (c) 2100 °C; the grain boundaries (black) were reconstructed and white areas show where indexing failed, which was most likely due to nano-sized grains and porosity.

slightly finer grained (Kirchhofer et al., 2013). This might be due to either the higher deposition temperature or the differing batch sizes of the two coating facilities. No obvious change in the grain shape was noted upon annealing. Small variations in the average grain size were found, but these were minor and contrary to other studies (van Rooyen et al., 2012) there was no consistent grain growth with increasing annealing temperature.

Raman spectroscopy of the three samples revealed significant differences in their respective stoichiometry. Sample 1 shows bands relating to cubic (β-modification) SiC exclusively (Fig. 3a), whereas sample 2 and 3 clearly exhibited traces of second phase silicon shown by a wide band of low intensity with a centre at ~480 cm^{-1}. In addition, the broadness of the SiC bands and their low intensity indicate that sample 3 is of less crystallinity than the other two (Fig. 3b). After thermal treatment the spectra of all samples showed the development of peaks proving the formation of thin graphitic sheets of carbon on the specimen surface as well as in the polished cross-section. These carbon bands appeared after annealing at 1600 °C and became more intense with increasing treatment temperature. This observation was taken as an additional prove that evaporation of SiC had occurred. Even much below its decomposition point (2700 °C), a vapour phase is formed above silicon carbide with silicon possessing the highest vapour pressure thus leaving the solid in excess of carbon (Gröbner et al., 1996). These carbon bands could be detected throughout the complete coating thickness proving that the evaporation process was not limited to the specimen surface, but also occurred on the grain surface within the coating.

Raman spectra of samples annealed at the highest treatment temperatures indicated the existence of hexagonal SiC (α-modification). For sample 1 and 2 α-SiC was found within the β-SiC matrix in some areas, but the content appeared low (Fig. 3a grey spectrum). In TEM investigations of SiC coatings other researchers identified the presence of some α-SiC content after annealing at 2100 °C (van Rooyen et al., 2010). In sample 3 the intensity and sharpness of the bands increased with annealing temperature leading to a separation of the bands into distinguishable peaks. After this crystallisation process α- and β-SiC were present and the ratio of their respective peaks varied depending on the exact measurement locations (Fig. 3b, blue and grey spectrum were taken on different locations in the same sample). The wide peaks indication some second phase amorphous silicon in sample 2 and 3 disappeared after annealing. Therefore some sharp peaks of crystalline silicon (520 cm^{-1}) were found in some locations of those two samples.

The XRD patterns collected on sample 1 and 2 showed all main peaks related to β-SiC and peak intensities and ratios did not change after thermal treatment (patterns not shown here). The presence of silicon was not visible in the XRD patterns, thus indicating that its content within the main SiC phase was low. In the pattern of sample 3 the peaks are weaker in the as deposited state and the peak width reduces consistently after annealing at increasing temperatures as expected in a crystallisation process (see Fig. 4). Weak peaks indicating the presence of α-SiC were observed after annealing at 2100 °C or more, those were not obvious in the other samples, leading to the conclusion that the α-SiC content is significantly higher in sample 3 than 1 or 2.

3.2. Mechanical properties

Weibull plots depicting the fracture strength of the freestanding SiC shells show that there is an immense variation between the three samples (Fig. 5). In its pristine state sample 1 exhibits an exceptionally high value of 1277 MPa, which is twice the fracture strength compared with the other two samples and higher than most literature data (Hong et al., 2007; Zhang et al., 2013). The variation of the individual strength values is acceptable, leading to a Weibull modulus of 7, which is higher than the value of 6 currently used in HTR fuel modelling codes (Miller et al., 2003). A reduction of the fracture strength occurs after thermal treatment, however the exact treatment temperature appears not to have an effect for sample 1 and the fracture strength is reduced to ~800 MPa irrespective of the actual annealing temperature of 1600, 1800 or 2000 °C. Due to the obvious layer thinning setting in from 2100 °C, the crush test was not applied on specimens treated beyond 2000 °C.

Sample 2 and 3 possess a significantly lower fracture strength of ~500 MPa and equally the variation within each set of samples is larger, leading to lower values for the Weibull modulus with ~4 and 2, respectively. Both sample showed some reduction in the fracture strength after being annealed at 1600 °C, which was more

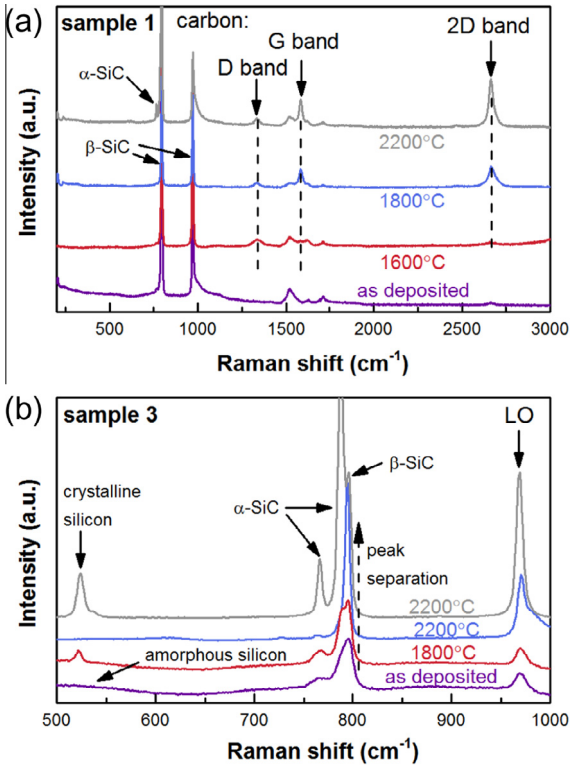

Fig. 3. Raman spectra taken on (a) the surface of sample 1 and (b) cross-section of sample 3.

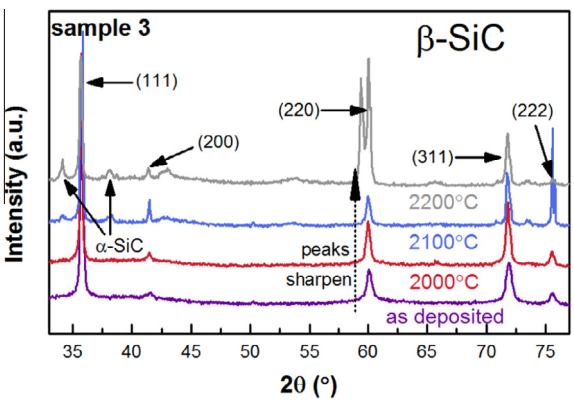

Fig. 4. XRD patterns collected of sample 3 as deposited and after thermal treatment.

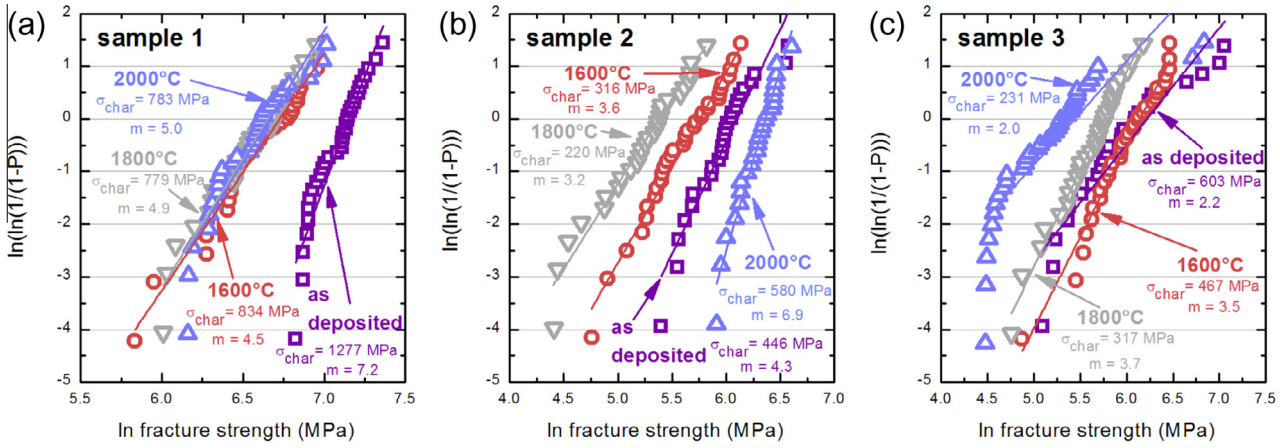

Fig. 5. Weibull plots of fracture strength of the SiC shells after thermal treatment, sample 3 had strong layer migration after annealing at 2000 °C and the data is only shown for comparison.

severe after 1800 °C treatment. In sample 3 significant changes in the specimen shape had occurred after annealing at 2000 °C, hence the analysis is not fully correct and the data is shown for comparison only. In sample 2 however a significant increase in the fracture strength was observed in the 2000 °C annealed samples. The characteristic fracture strength was increased to 580 MPa, which was higher than the 446 MPa measured in the specimens in the as deposited state.

The reasons for the observed changes in the strength values are not unambiguously clear. The porosity content was found to be highly dependent on the annealing temperature, whereas the crush test results of sample 1 appear to be unrelated to the actual treatment temperature, thus suggesting that porosity plays a subordinate role. This confirms observations from previous studies that found only slightly decreased strength values after short annealing at 2000 °C (Zhang et al., 2013) or even 2100 °C (van Rooyen et al., 2010). Oxidation effects are excluded, since thermal treatment was conducted in argon atmosphere in a graphite environment and there were no visible signs for degradation due to oxidation. However, the presence of silicon with its low melting point (1420 °C) is known to have a strongly detrimental effect for high temperature mechanical performance of SiC. Its crystallisation and potential evaporation will affect the SiC integrity, which might be the cause for the more pronounced weakening observed in sample 2 and 3 after the treatment temperature increased from 1600 to 1800 °C. The pronounced increase of the fracture strength in sample 2 upon a further raise in temperature to 2000 °C might be related to the precipitation of SiC, which acts as some flaw healing mechanism. The inner surface of the SiC coatings had been investigated by SEM, changes were not easily visible, but it is possible that thermal treatment had some effect that lead to the lower fracture strength observed in the annealed specimens of sample 1 and the changing fracture strength in sample 2 and 3.

The values of elastic modulus and hardness were determined as an average of at least 30 indents taken on different particles for each sample and condition. Nanoindentation experiments conducted at room temperature showed some variation in the elastic modulus for the different samples (Fig. 6b), however the hardness is almost identical (Fig. 6a). The values were found to compare well with prior nanoindentation studies (Hosemann et al., 2013; López-Honorato et al., 2008; Tan et al., 2009). For the elastic modulus a large range of ~200 to 400 GPa has been reported and the hardness can vary between 30 and more than 40 GPa.

Annealing the samples did not have an obvious detrimental effect. There is a slight decrease between the elastic modulus measured after annealing 1600 °C and 1800 °C in sample 1, but above

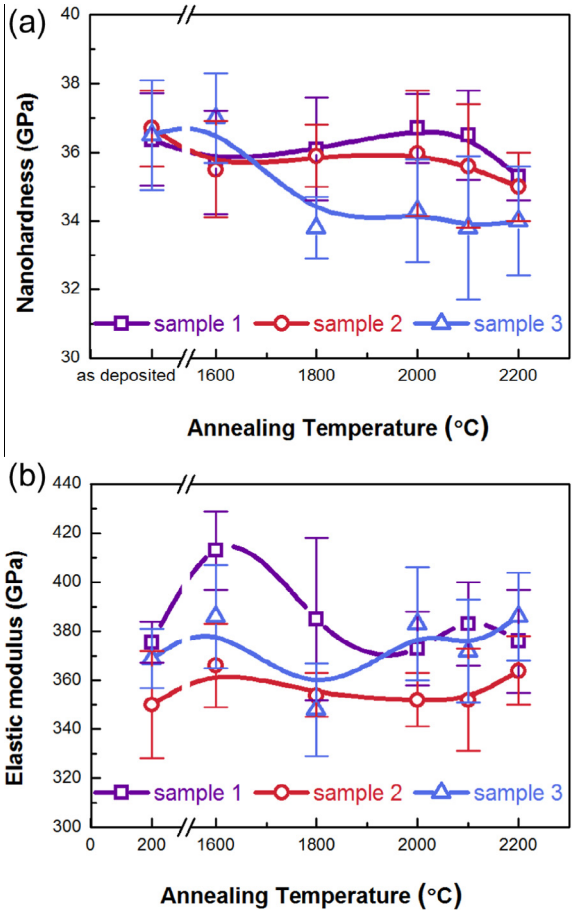

Fig. 6. Plots of (a) hardness and (b) elastic modulus as determined by nanoindentation after annealing experiments.

even up to the highest annealing temperatures the values for the elastic modulus are well within the standard deviation of the measurement. The hardness was found to remain constant for sample 1 and 2 over the whole temperature range, for sample 3 however it drops after annealing at 1800 °C and remains constant from there onwards. This might be a reflection of the more pronounced microstructural changes described earlier in sample 3. The small silicon content in sample 2 does not show a measurable impact on the hardness after annealing. The observed porosity formation,

even though significant is not reflected in the values obtained by nanoindentation here, which is probably due to the small measurement volume.

Using a nanoindentation facility capable of conducting measurements at elevated temperatures the elastic modulus and hardness of sample 1 were measured up to a maximum temperature of 500 °C. Comparable tests were conducted on a bulk CVD SiC piece to exclude potential effects caused by the embedding required for measuring the TRISO particles and both data plots are displayed in Fig. 7. Overall, the results compared favourable with each other. The hardness shows a continuous decrease over the measured temperature range, which was reduced from 36 GPa at room temperature to 23 GPa at 500 °C in the TRISO coating and 20 GPa in the bulk CVD SiC piece. The bulk CVD SiC possesses a grain size that is about one magnitude larger than the TRISO coating, which could be the reason for the more pronounced drop in hardness.

The decrease of the elastic modulus with temperature is only minor. Some reduction with temperature is expected due to a decrease of the stiffness of the atomic bonds, but this effect is small. Raman spectroscopy can determine the elastic modulus evolution with temperature if the specimen is placed on a hot stage (Zhao et al., 2011). The temperature evolution of the elastic modulus was measured using this approach for sample 1 and the results were added to Fig. 7b. The curve shows a flat decrease of the elastic modulus with temperature. Raman spectroscopy does not reflect microstructural features such as grain boundaries or porosity, so the obtained values are overall higher, however the temperature dependency determined is comparable with the nanoindentation results thus verifying their validity.

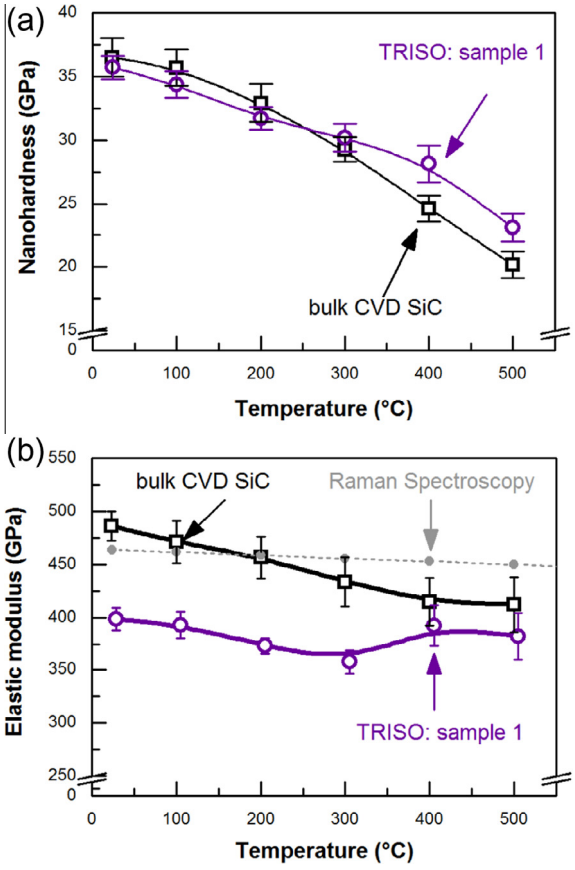

Fig. 7. Evolution of hardness and elastic modulus with temperature as measured in sample 1 and a bulk CVD SiC sample by high temperature nanoindentation.

4. Summary

The first signs of SiC disintegration are seen after annealing in low-pressure, inert atmosphere at 1600 °C by the formation of graphitic sheet on the sample surface, which occurs irrespective of the sample stoichiometry. With increasing treatment temperature porosity is formed throughout the SiC coating and from 2100 °C onwards layer thinning can be observed. Due to precipitation new SiC crystals consisting of large grains were found to form on the specimen surface at temperatures above 2000 °C. Within the coating no grain growth could be detected and non-cubic SiC was identified after annealing at 2100 °C or beyond. SiC of insufficient crystallinity undergoes a crystallisation process leading to the formation of α and β-SiC.

The fracture strength measurements identified a very high value for stoichiometric SiC (sample 1) that was somewhat reduced after thermal treatment. The samples containing second phase silicon had a lower strength in their as-deposited state and showed further reduction after thermal treatment. However, despite the immense microstructural changes the elastic modulus and hardness as measured by nanoindentation were not impaired significantly by the thermal treatment.

5. Conclusion

Stoichiometric SiC retains its mechanical integrity remarkably well after short-term exposure at extreme temperatures even beyond 1600 °C. Although evaporation of SiC causes porosity formation the mechanical properties as measured by crush test and nanoindentation are only slightly impaired, thus mechanical failure of SiC due to temperature effects alone appears unlikely. In addition, in TRISO fuel SiC evaporation is suppressed by the OPyC layer, thus porosity formation that could potentially provide a migration pathway for fission products is impeded.

The initial results from the high temperature nanoindentation tests are very encouraging. Measurement uncertainty was acceptable and the obtained values were well within the expected range. Continuing development of this technique will allow evaluating also other influencing factors as e.g. irradiation impact.

Acknowledgements

This work has been funded by the EPSRC (EP/J021172/1 and EP/L018616/1) and the European Commission through the FP7 Archer project (Contract No. 269892).

All research data supporting this publication are directly available within this publication.

References

Byun, T.S., Hunn, J.D., Miller, J.H., Snead, L.L., Kim, J.W., 2010. Evaluation of fracture stress for the SiC layer of TRISO-coated fuel particles using a modified crush test method. Int. J. Appl. Ceram. Technol. 7 (3), 327–337.

Gröbner, J., Lukas, H.L., Aldinger, F., 1996. Thermodynamic calculation of the ternary system Al-Si-C. Calphad 20, 247–254.

Hancke, J.J., van Rooyen, G.T., de Villiers, J.P.R., 2013. The effect of coating parameters and annealing on the crushing strength of TRISO coated particles. Nucl. Technol. 182 (1), 49–56.

Hong, S.G., Byun, T.S., Lowden, R.A., Snead, L.L., Katoh, Y., 2007. Evaluation of the fracture strength for silicon carbide layers in the tri-isotropic-coated fuel particle. J. Am. Ceram. Soc. 90 (1), 184–191.

Hosemann, P., Martos, J.N., Frazer, D., Vasudevamurthy, G., Byun, T.S., Hunn, J.D., Jolly, B.C., Terrani, K., Okuniewski, M., 2013. Mechanical characteristics of SiC coating layer in TRISO fuel particles. J. Nucl. Mater. 442 (1), 133–142.

Ikawa, K., Kobayashi, F., Iwamoto, K., 1978. Failure of coated fuel particles during thermal excursion above 2000 °C. J. Nucl. Sci. Technol. 15 (10), 774–779.

Kirchhofer, R., Hunn, J.D., Demkowicz, P.A., Cole, J.I., Gorman, B.P., 2013. Microstructure of TRISO coated particles from the AGR-1 experiment: SiC grain size and grain boundary character. J. Nucl. Mater. 432 (1), 127–134.

López-Honorato, E., Meadows, P.J., Tan, J., Xiao, P., 2008. Control of stoichiometry, microstructure, and mechanical properties in SiC coatings produced by fluidized bed chemical vapor deposition. J. Mater. Res. 23 (6), 1785–1796.
López-Honorato, E., Tan, J., Meadows, P.J., Marsh, G., Xiao, P., 2009. TRISO coated fuel particles with enhanced SiC properties. J. Nucl. Mater. 392 (2), 219–224.
Miller, G.K., Petti, D.A., Varacalle Jr., D.J., Maki, J.T., 2003. Statistical approach and benchmarking for modeling of multi-dimensional behavior in TRISO-coated fuel particles. J. Nucl. Mater. 317 (1), 69–82.
Minato, K., Fukuda, K., 1991. Strength and Young's modulus of silicon carbide layers of HTGR fuel particles at high temperatures. J. Nucl. Mater. 182, 6–10.
Ogawa, T., Ikawa, K., 1981. Crushing strengths of SiC-TRISO and ZrC-TRISO coated fuel particles. J. Nucl. Mater. 98 (1), 18–26.
Oliver, W.C., Pharr, G., Pharr, G.M., 1992. An improved technique for determining hardness and elastic-modulus using load and displacement sensing indentation experiments. J. Mater. Res. 7 (6), 1564–1583.
Rooyen, I.J., Dunzik-Gougar, M.L., van Rooyen, P.M., Trowbridge, T., 2012. On techniques to characterize and correlate grain size, grain boundary orientation and the strength of the SiC layer of TRISO coated particles: a preliminary study. In: Presented at the HTR 2012, Tokyo, pp. 1–12.
Tan, J., Meadows, P.J., Zhang, D., Chen, X., López-Honorato, E., Zhao, X., Yang, F., Abram, T.J., Xiao, P., 2009. Young's modulus measurements of SiC coatings on spherical particles by using nanoindentation. J. Nucl. Mater. 393 (1), 22–29.
van Rooyen, I.J., Neethling, J.H., van Rooyen, P.M., 2010. The influence of annealing temperature on the strength of TRISO coated particles. J. Nucl. Mater. 402 (2), 136–146.
van Rooyen, I.J., Neethling, J., Henry, A., Janzén, E., 2010. Influence of phosphorous and high temperature annealing on the nanostructures of 3C-SiC. In: Presented at the HTR 2010.
van Rooyen, I.J., Neethling, J.H., Henry, A., Janzén, E., Mokoduwe, S.M., van Vuuren, A.J., Olivier, E.J., 2012. Effects of phosphorous-doping and high temperature annealing on CVD grown 3C-SiC. Nucl. Eng. Des. 251, 191–202.
Verfondern, K., 2011. Advances in HTR Fuel Technology. IAEA.
Zhang, H., López-Honorato, E., Xiao, P., 2013. Effect of thermal treatment on microstructure and fracture strength of SiC coatings. J. Am. Ceram. Soc. 96 (5), 1610–1616.
Zhao, X., Yang, F., Zhang, H., Xiao, P., 2011. Nondestructive evaluation of high-temperature elastic modulus of 3C-SiC using Raman scattering. J. Raman Spectrosc. 43 (7), 945–948.